Angle-Dependent Terahertz Time-Domain Spectroscopy of Amino Acid Single Crystals

Rakchanok Rungsawang,† Yuko Ueno, Isao Tomita, and Katsuhiro Ajito*

NTT Basic Research Laboratories, 3-1 Morinosato-Wakamiya, Atsugi, Kanagawa 243-0198, Japan

Received: January 24, 2006; In Final Form: May 25, 2006

The measurement of absorption spectra using angle-dependent terahertz (THz) time-domain spectroscopy for amino acid single crystals of L-cysteine and L-histidine is reported for the first time. Linearly polarized THz radiation enables us to observe angle-dependent far-infrared absorption spectra of amino acid single crystals and determine the direction of the oscillating dipole of the molecules in the 20−100 cm^{-1} range. By comparing the THz spectra of a single crystal and powder, we found that there was a clear hydrogen-bond peak in the crystal spectrum as a result of the larger hydrogen-bond network. The low-temperature THz spectra of amino acid microcrystals showed more intermolecular vibrational modes than those measured at room temperature. An ab initio frequency calculation of a single amino acid molecule was used to predict the intramolecular vibrational modes. The validity of the calculation models was confirmed by comparing the results with experimentally obtained data in the Raman spectral region.

1. Introduction

Terahertz time-domain spectroscopy (THz-TDS) has been a useful tool in physics and chemistry for studying a wide variety of different samples in the 0.1−3.0 THz (∼3−100 cm^{-1}) region, the lower end of the far-infrared region.[1−12] Low-frequency vibrational modes of molecules, such as torsional and collective vibrational modes and hydrogen-bond modes, exist in the region.[3,4] This technique allows the electric field of a repetitive pulse of THz radiation to be measured directly, thus yielding complex dielectric constants.[5,6] The electric field is coherent detected with subpicosecond temporal resolution using femtosecond laser pulses.[13,14] Therefore, THz-TDS provides a high signal-to-noise ratio as compared to the low-energy photon detector used for Fourier transform infrared spectroscopy. The polarization of the THz radiation is well defined because the radiation is generated by using a laser as a pumping source. Many biological molecules, such as DNA components, polypeptides, and amino acids, have been investigated below 100 cm^{-1} using THz-TDS and powder form samples.[3,4,7−10] The THz-TDS technique requires a sample that is larger than a THz beam. Typically, samples are made by pressing micrometer-size polycrystalline powders into a pellet. As a result, the THz absorption spectrum of the powder reflects the average properties of randomly orientated molecules. Recently, single crystals of highly explosive materials were observed in transmitted spectra obtained using THz-TDS.[11] The results show that THz spectra obtained at different crystal faces are not identical due to their dependence projection of the dipole derivative of the mode onto the direction of the THz polarization.

Low-frequency vibrational spectra of some amino acids at different crystal faces have been obtained with a variety of techniques, that is, Fourier transform spectroscopy, Mandelshtam−Brillouin spectroscopy, and Raman scattering, with a view for observing absorption features in the 0.2−400 cm^{-1} range.[15] However, the spectrum of a rotationally oriented amino acid single crystal has not yet been studied. The amino acid molecules occur in the crystal in dipolar ion (zwitterion) form. Many amino acid crystals are formed from relatively independent sublattices linked by hydrogen intermolecular bonds between amine hydrogen atoms and carboxylate oxygen atoms.[16] The molecules are ordered with hydrogen bonds in the amino acids crystals. Far-infrared spectra of polycrystalline amino acid powder have been observed by Fourier transform spectroscopy[17] and THz-TDS.[2,9,12] However, the relationship between molecular orientation and hydrogen bonding has not been investigated.

In this paper, we report on the measurement of THz absorption spectra using angle-dependent THz-TDS for amino acid single crystals of cysteine and histidine. Linearly polarized THz radiation with a rotation stage and a submillimeter metal aperture in a THz-TDS spectrometer enables us to observe angular-dependent THz spectra of amino acid single crystals and determine the direction of the oscillating dipole of the molecules in the crystals. The THz spectra of the single crystals were compared to those obtained with randomly oriented microcrystal powder. The difference between the crystal and powder THz spectra revealed absorption due to hydrogen bonds. The THz spectra of the powder samples were also measured at low temperature to determine the characteristics of the absorption peaks of the microcrystals. The ab initio frequency calculation of a single molecule in the gas phase is widely used to predict vibrational modes in infrared and Raman spectra.[18,19] The low vibrational frequencies of some molecules can be found in the frequency region that THz-TDS may be used to verify. We performed an ab initio calculation to predict the intramolecular vibrational modes of the amino acids. The validity of the calculation model was confirmed by comparing the results obtained in the Raman spectral region.

2. Experimental Section

The terahertz spectroscopy was performed using a commercially available THz-TDS spectrometer (THz-TDS2004, Aispec), a 100-fs duration pulse of 800 mm light from a femtosecond laser (Vitesse, Coherent), and an additional rotation stage for angle-dependent THz absorption spectroscopy as

* Corresponding author. Tel.: +81-46-240-3565. Fax: +81-46-270-2364. E-mail: ajito@nttbrl.jp.

† Present address: Semiconductor Physics Group, Cavendish Laboratory, JJ Thomson Ave., Cambridge CB3 0HE, U.K. E-mail: rr333@cam.ac.uk.

10.1021/jp060492n CCC: $33.50
Published on Web 09/29/2006

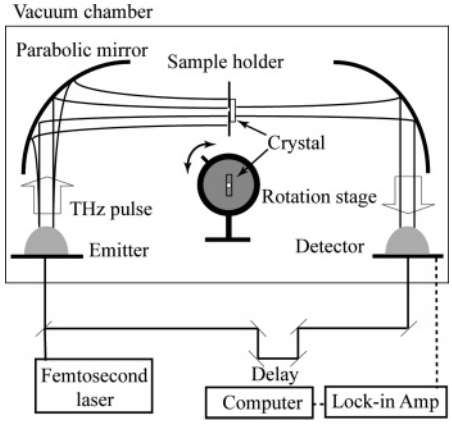

Figure 1. Schematic of angle-dependent THz-TDS system. The emitter and detector are photoconductive antennas. The sample holder is composed of a rotation stage with an aluminum plate inside. The THz beam was transmitted in a vacuum chamber.

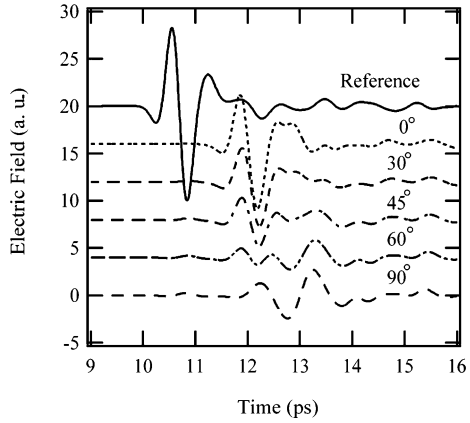

Figure 2. Transmitted THz signals after they had passed through the 0.5-mm metal aperture (solid line) and the cysteine single crystal at various angles (dashed lines). 0° is defined when the *c*-axis of the crystal is parallel to the polarization of the THz field. The waveforms are vertically offset.

shown in Figure 1. The spectrometer includes photoconductive antennas for the generation and detection of THz pulses. The laser light was separated into two beams. One beam was used to generate photocarriers on a low-temperature-grown GaAs (LT-GaAs) emitter. The photocarriers were accelerated by applying a bias voltage to micro-gap electrodes on an LT-GaAs wafer, giving rise to an output THz electromagnetic pulse. The THz radiation was then collimated to a parabolic mirror with a hemispherical silicon lens. We adopted a rotation stage with a 0.5-mm diameter aperture at the center of an aluminum plate as a sample holder for measuring the angle-dependent THz spectrum of a single crystal. The rotation angle of the stage was accurate to 5°. The sample holder was placed at the focus of the parabolic mirror. The emitted THz pulses were at broadband frequencies ranging from 3.33 cm^{-1} (0.1 THz) to 133.33 cm^{-1} (4.0 THz). Long wavelengths were blocked by the metal aperture. As a result, there was a sharp dip in the THz spectrum at 7.24 cm^{-1}. We avoided this dip and adjacent side effects by considering the THz spectrum from 20 cm^{-1}. The sample crystal was attached centrally on the rear of the holder. In other words, the THz beam passed through the aperture before reaching the sample. The beam that passed through the sample was collected by another parabolic mirror and sent to the photoconductive detector. Photocarriers at the detector, generated by the femtosecond pulses, were driven by the THz electric field, resulting in current flows. We detected a voltage that was linearly proportional to the electric field strength. The S/N ratio of our system was approximately 60 dB. Powder samples pressed into pellets were detected using a 5-mm diameter metal plate. The samples were inserted into a cryostat in a low-temperature apparatus in a liquid nitrogen flow.

Near-infrared Raman spectroscopy of the amino acid crystals was employed to verify the calculated results obtained in the Raman region. The laser light source was a cw Ti:-sapphire (Titan-Cw, Schwartz Electrooptics) with a frequency of 730 nm. A commercially available Raman microprobe spectrometer (Ramascope, Renishaw) was specially modified for NIR laser light.[20] The spectral resolution of the system was 1 cm^{-1}.

L-Cysteine and L-histidine were purchased from Wako Pure Chemical Industries Ltd. The cysteine crystal was recrystallized with water, while the histidine was used without any further chemical processing. Both crystals have orthorhombic structures, which were identified by the X-ray diffraction method. The dimensions of the cysteine and histidine crystals were 0.3 × 0.5 × 1.65 mm^3 and 0.5 × 0.65 × 4.5 mm^3, respectively. By using an X-ray crystallography examination, we found the longest directions of the crystals to be the *c*-axis for the cysteine crystal and the *a*-axis for the histidine crystal. To obtain powder samples, the purchased amino acids were crushed and mixed with polyethylene powder at 20 wt %. The mixture was compressed into a pellet at 80 kgf/cm^2. The reference waveform was detected when the THz pulses passed through the empty aperture. The apparatus was operated under a pressure of 50 Pa to avoid water vapor absorption peaks. The transmitted THz pulses were measured 16 times for one sample condition. The 0° angle was defined so that the long direction of the crystals was parallel to the THz field polarization. The crystal was rotated at certain angles between 0° and 90°.

3. Computations

We calculated the vibrational frequencies of isolated cysteine and histidine molecules using the Gaussian 03 software package to enable us to assign absorption peaks in the low-frequency region.[21] Zwitterionic forms of the molecules were used by starting with the structures obtained from experimental neutron diffraction and X-ray crystallographic data.[22,23] We optimized the molecule geometry and then calculated infrared and Raman spectra at the HF/6-31* level. It should be noted that frequency calculations based on density function theory usually have a smaller error than the Hartree−Fock calculation but the zwitterionic form is not retained after optimization. Therefore, we scaled the frequency results with an empirical factor of 0.8929.[24]

4. Results

4.1. Cysteine. The temporal waveform of the reference THz pulse that passed through the 0.5-mm metal aperture is shown as a solid line in Figure 2. When the pulse passed through the aperture and a crystal, the absorption of the sample introduced a pulse delay and changes in the waveform. The waveforms of THz pulses transmitted through the cysteine single crystal at different angles from 0° to 90° are shown as dashed lines in the same figure. The THz pulse that passed through the crystal axis aligned at 90° to the THz polarization diverged greatly from the reference pulse because of the high absorption. Figure 3a shows THz absorption spectra of the cysteine crystal measured at room temperature in the 20−100 cm^{-1} range, which correspond to the temporal waveforms of THz pulses shown in Figure 2. The spectral resolution was 0.24 cm^{-1} determined by a temporal resolution of 4.2 fs and a data point number of

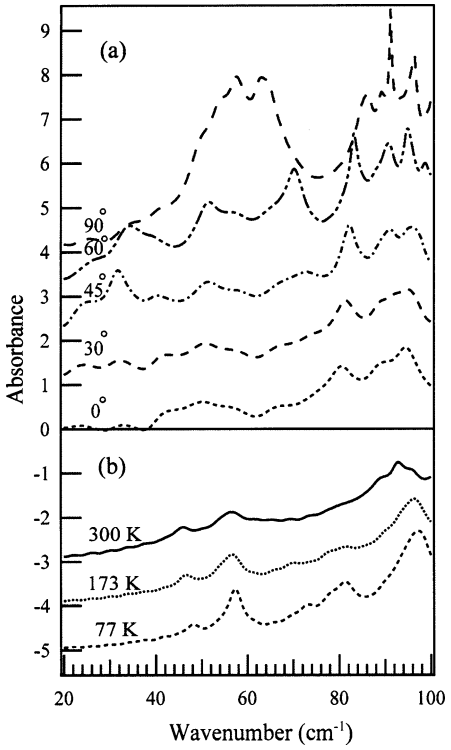

Figure 3. (a) Absorbance of cysteine single crystal at different angles (dashed lines) and (b) powder at room temperature (−), 173 K (· · ·), and 77 K (- - -). 0° is defined when the *c*-axis of the crystal is parallel to the polarization of the THz field. The spectra are vertically offset.

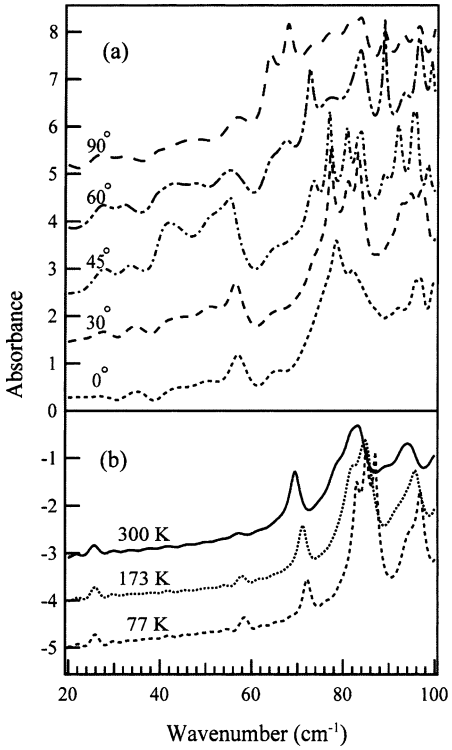

Figure 4. (a) Absorbance of histidine single crystal at different angles (dashed lines) and (b) powder at room temperature (−), 173 K (· · ·), and 77 K (- - -). 0° is defined when the *a*-axis of the crystal is parallel to the THz field polarization. The spectra are vertically offset.

32 768. The THz spectrum of the crystal at 90° has no meaning above 85 cm^{-1} because of high absorbance and darkness of high-frequency components. In the same spectrum, the absorption between 54 and 64 cm^{-1} is too high, with a transmittance of less than 0.02%, and therefore the spectral region can be easily contaminated by noise. As a result, the peaks at 57.64 and 63.43 cm^{-1} are not reliable. However, the broad absorption band between 50 and 70 cm^{-1} was reproduced in different scans. Significantly, the peak at 80.50 cm^{-1} of the crystal spectra at 0° was shifted in the higher frequency direction and became sharper when the angle between the crystal and the THz polarization was increased. This result indicates that angle-dependent THz-TDS is sensitive to the molecular orientation in the crystals. Figure 3b shows a series of temperature-dependent THz spectra of microcrystalline cysteine mixed with polyethylene powder. The peak intensities in the powder spectrum at low temperature were larger and sharper than those at room temperature. We suggest that the peak shift is related to intermolecular interactions, that is, hydrogen bonds or the van der Waals force, which are stronger at low temperature, and the temperature was insufficiently low to induce a peak shift originating from a torsion or deformation skeleton.[9] The powder peak at 81.28 cm^{-1} exists at 77 K, corresponding to the peaks in the crystal spectra at 0−60°. The peak at 70.18 cm^{-1} seen in the powder spectrum at 173 K is also observed in the crystal spectra at 45° and 60°. We found that the peak at 46.06 cm^{-1} observed for the powder does not appear in the single-crystal spectra.

4.2. Histidine. Figure 4a and b shows THz absorption spectra of the histidine single crystal at a variety of angles and of histidine powder, respectively. The peak at 28.56 cm^{-1} clearly appears at angles of 45° and 60°. The peak at 57 cm^{-1} in the crystal was also found as a small peak in the powder spectrum at room temperature. The powder peak at 69.46 cm^{-1} at room temperature might be related to the crystal peak at 90° that appears at 68 cm^{-1}. When the powder sample was cooled, the peaks above 50 cm^{-1} had blue shifts, while the peak at 25.56 cm^{-1} did not.

5. Discussion

5.1. Cysteine. From the angular dependence of cysteine spectra, we found that the absorption peak at 46.06 cm^{-1} did not appear in the crystal spectra. There are two possible explanations for this. This vibration mode might be related to the peaks found at around 50 cm^{-1} in the crystal spectra. Alternatively, the frequency might exist if the cross-sectional surface rather than the longitudinal side of the crystal is irradiated by the THz field. The changes in the peak features around 80 cm^{-1} with increasing rotation angle are similar to those in the alanine absorption peak caused by the strengthening of the hydrogen bond with decreasing temperature.[25] The powder peak related to this absorption is weak at room temperature but formed as the temperature decreased. The powder peak around 80 cm^{-1} can be assigned as a hydrogen-bond network for two reasons. The peak is stronger in the larger crystal and shifts to a higher frequency when the network shrinks at low temperature. The powder peak around 70 cm^{-1} that existed at low temperatures and in crystal spectra can be ascribed as having the same origin.

The theoretical vibrational frequencies of a single cysteine molecule are shown and compared to experimentally obtained Raman data and THz-TDS data in Table 1. There are 36 vibrational modes. The calculated results agree well with those reported in the literature.[19] The Raman peaks in Table 1 were observed when the *c*-axis of the cysteine crystal was perpendicular to the laser light polarization. We found that peak intensities of the Raman spectra changed when the angle between the crystal axis and the light polarization was varied,

TABLE 1: Calculated and Experimental Frequencies of Cysteine

	experiment		
	Raman		
calculated	this paper	ref 19	TDS
			46.06
55			56.67
			92.85
115			
		169	
186	211	212	
256	269	268	
271			
		301	
337			
343			
351	369	364	
	446	443	
506	538	536	
581	642	639	
	696	692	
721	757	756	
733	776	773	
795	807	807	
837	825	822	
867	871	869	
960	943	942	
1010	1005	1001	
1049	1069	1061	
1100	1111	1105	
1188	1203	1199	
1275	1267	1267	
1291	1305	1295	
1322			
1356	1354	1354	
1374	1400	1397	
1455	1427	1424	
1590	1575	1574	
1638		1611	
1770	1624	1644	
2618	2550	2546	
2697			
2881			
2928	2959	2970	
2947	3001	3000	
3317		3190	
3391			

but the results are not shown here. To verify the calculation model, we compared the Raman spectrum with that of ref 19, which used 1064-nm excited light with a resolution of 4 cm^{-1}. Although the molecule was assumed to be in a vacuum in the calculation model, the results could predict the vibrational modes of a single molecule in the Raman spectra.[22] The lowest frequency mode of the calculated results, 55 cm^{-1}, agrees with the value of 56.67 cm^{-1} in the powder spectrum at room temperature. This peak is sharper and stronger at low temperature but shifted only by 0.73 cm^{-1}. The changes in this absorption mode are different from the others, which are due to hydrogen bonds. The small peak shift may originate from the presence of sulfur atoms and related hydrogen bonds. It is predicted to be the torsional mode of the carboxylate group. Calculated atomic displacements in the vibrational mode obtained with the VLX program are shown in Figure 5a.[26] The direction of the oscillating dipole of this mode was perpendicular to the *c*-axis. This is in good agreement with the experimentally observed strong absorption band around 60 cm^{-1} when the THz field was applied perpendicularly to the *c*-axis. The broadening of the peak might indicate the effect of a mode that is strongly coupled to neighboring atoms and hydrogen bonds. It should be noted that the calculation model might accurately predict more vibrational modes in the low-frequency region if the molecule is simulated in periodic structures.

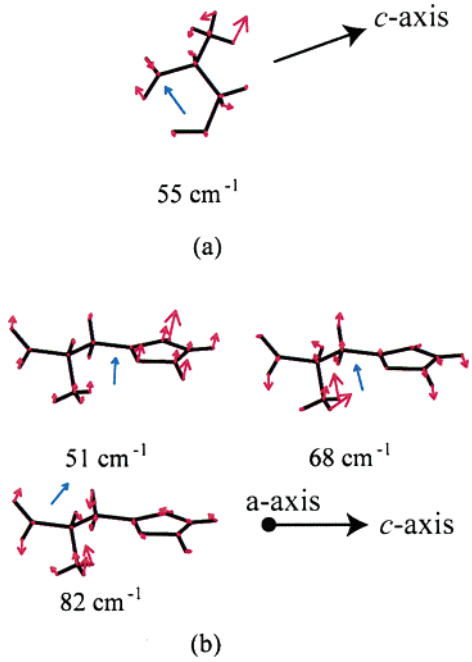

Figure 5. Atom displacements calculated at the HF-6-31G* level for cysteine (a) and histidine molecules (b). The black arrows show the direction of the *c*-axis, modified from X-ray data in ref 27 for cysteine and ref 23 for histidine, while the blue arrows show the direction of oscillating dipoles obtained from the calculation.

5.2. Histidine. The histidine molecule is more complex than the cysteine molecule due to the presence of an imidazole ring. In addition to intermolecular hydrogen bonds, there are intramolecular hydrogen bonds between the nitrogen atom on the imidazole side and the hydrogen atom in the amino group. These are assumed to be observable in the THz spectrum. The peak at 57 cm^{-1} in the crystal spectra was assigned as a hydrogen bond for the same reason as that described for the cysteine results. We simulated the vibrational frequencies of isolated histidine molecules in a vacuum at the HF/6-31G* level. Table 2 lists 54 possible vibrational modes of this single molecule. The lowest three vibrational modes, 51, 68, and 82 cm^{-1}, are assigned as torsional vibration, as shown in Figure 5b. Two absorption peaks observed using THz-TDS, 69.46 and 83.20 cm^{-1}, are equivalent to the later torsional modes. However, we found that these peaks shifted when the temperature was decreased as seen in Figure 4b and the 83.4 cm^{-1} peak appeared at all angles. The histidine calculation model cannot be used to predict low-frequency vibrational modes properly. Resonance contributions in the imidazole ring may cause the calculation model to fail when using single molecules. Although the calculation cannot predict vibrational frequencies precisely, it indicates that the directions of the oscillating dipole of the three lowest modes are nearly perpendicular to the *a*-axis. This can explain why the absorption is relatively high at 90°. By comparison with the data provided in ref 15 and shown in Table 2, it is clear that Raman spectroscopy can reveal more absorption peaks in the low-frequency region. Some peaks in the Raman spectrum were observed in a single histidine crystal using THz-TDS, including those of 41 cm^{-1} at 45° and 64 cm^{-1} at 90°. Interestingly, the powder peak at 25.56 cm^{-1} is weak and remains unchanged with decreasing temperature. It has already been assigned as a torsional vibration mode.[17]

TABLE 2: Calculated and Experimental Frequencies of Histidine

experiment					experiment
	Raman				Raman
calculated	this paper	ref 15	TDS	calculated	this paper
		6		651	659
		12		709	683
		16		771	733
		26	25.56	785	787
		31		811	808
		37			827
		41		878	855
		45		884	
51				916	920
		55	57.40	921	935
		64		951	966
68			69.46	1018	978
		73		1043	
		76		1062	1063
82		82	83.20	1101	1090
		86	89.23	1113	1114
		95	94.30		1142
		105		1201	1177
		111		1228	1226
		120		1234	1252
		127		1256	1273
131		130		1214	1320
		135		1330	1338
144		141		1350	1350
		150		1382	1382
		158		1411	1409
		168		1443	1432
		176		1449	1479
		180		1517	1501
		183		1577	1574
		186		1586	1612
205		190		1654	1643
	215	219		1761	
	243	240		2846	2839
280	289	257		2921	2900
311	318			2961	2974
	338			3081	
353	365			3100	3132
431	406			3139	3150
494				3320	
512	542			3374	
602				3495	
632	629				

6. Conclusion

The angle-dependent THz spectra of L-cysteine and L-histidine single crystals measured with THz-TDS were reported for the first time. We studied orientated molecules to determine the direction of the oscillating dipole for the absorption peaks. By comparing the THz spectra of a single crystal and powder, we found that there was a clear hydrogen-bond peak in the crystal spectrum as a result of the larger hydrogen-bond network. The powder spectra measured at low temperature showed more intermolecular vibrational modes than those measured at room temperature. Simulation results for two amino acids indicated the directions of oscillating dipoles of low-frequency vibrational modes. These provide high absorption when molecules are probed by a THz electric field whose polarization is parallel to the dipole directions.

Acknowledgment. We thank the Wakate Project at NTT for financial support, Dr. Keiichi Torimitsu at NTT for his encouragement, and Associate Professor Akira Sakamoto at Saitama University for fruitful discussions about the calculation methods.

References and Notes

(1) Grischkowsky, D. R.; Fattinger, Ch.; Exter, M. van; Keiding, S. R. *J. Opt. Soc. Am. B* **1990**, *7*, 2006−2015.
(2) Kojima, S.; Tsumura, N.; Takeda, W. M.; Nishizawa, S. *Phys. Rev. B* **2003**, *67*, 035102−035105.
(3) Yu, B.; Zeng, F.; Yang, Y.; Xing, Q.; Chechin, A.; Xin, X.; Zeylikovich, I.; Alfano, R. R. *Biophys. J.* **2004**, *86*, 1649−1654.
(4) Walther, M.; Plochocka, P.; Fischer, B.; Helm, H.; Jepsen, P. U. *Biopolymers* **2002**, *67*, 310−313.
(5) Kindt, J. T.; Schmuttenmaer, C. A. *J. Phys. Chem.* **1996**, *100*, 10373−10379.
(6) Zhang, J.; Grischkowsky, D. R. *J. Phys. Chem. B* **2005**, *108*, 18590−18600.
(7) Fischer, B. M.; Walther, M.; Jepsen, P. U. *Phys. Med. Biol.* **2002**, *47*, 3807−3814.
(8) Yamamoto, K.; Tominaga, K.; Sasakawa, H.; Tamura, A.; Murakami, H.; Ohtake, H.; Sarukura, N. *Biophys. J.* **2005**, *89*, L22−L24.
(9) Taday, P. F.; Bradley, I. V.; Arnone, D. D. *J. Biol. Phys.* **2003**, *29*, 109−115.
(10) Fischer, B. M.; Hoffmann, M.; Helm, H.; Wilk, R.; Rutz, F.; Kleine-Ostmann, T.; Koch, M.; Jepsen, P. U. *Opt. Express* **2005**, *13*, 5205−5215.
(11) Barber, J.; Hooks, D. E.; Funk, D. J.; Averitt, R. D.; Taylor, A. J.; Babikov, C. *J. Phys. Chem. A* **2005**, *109*, 3501−3505.
(12) Yamaguchi, M.; Miyamura, F.; Yamamoto, K.; Tani, M.; Hangyo, M. *Appl. Phys. Lett.* **2005**, *86*, 053903.
(13) Exter, M. van; Grischkowsky, D. R. *IEEE Trans. Microwave Theory Tech.* **1990**, *38*, 1684−1691.
(14) Wu, Q.; Zhang, X.-C. *Appl. Phys. Lett.* **1995**, *67*, 3523−3525.
(15) Dovbeshko, G.; Berezhinsky, L. *J. Mol. Struct.* **1998**, *450*, 121−128.
(16) Jonsson, P.-C.; Kvick, A. *Acta Crystallogr., Sect. B* **1972**, *28*, 1827−1833.
(17) Matei, A.; Drichko, N.; Gompf, A.; Dressel, M. *Chem. Phys.* **2005**, *316*, 61−71.
(18) Sakamoto, A.; Kuroda, M.; Harada, T.; Tasumi, M. *J. Mol. Struct.* **2005**, *735*−*736*, 3−9.
(19) Pawlukojc, A.; Leciejewicz, J.; Ramirez-Cuesta, A. J.; Nowicka-Scheibe, J. *Spectrochim. Acta, Part A* **2005**, *61*, 2474−2481.
(20) Ajito, K.; Torimitsu, K. *Trends Anal. Chem.* **2001**, *20*, 255−262.
(21) Frisch, M. J.; Trucks, G. W.; Schlegel, H. B.; Scuseria, G. E.; Robb, M. A.; Cheeseman, J. R.; Montgomery, J. A., Jr.; Vreven, T.; Kudin, K. N.; Burant, J. C.; Millam, J. M.; Iyengar, S. S.; Tomasi, J.; Barone, V.; Mennucci, B.; Cossi, M.; Scalmani, G.; Rega, N.; Petersson, G. A.; Nakatsuji, H.; Hada, M.; Ehara, M.; Toyota, K.; Fukuda, R.; Hasegawa, J.; Ishida, M.; Nakajima, T.; Honda, Y.; Kitao, O.; Nakai, H.; Klene, M.; Li, X.; Knox, J. E.; Hratchian, H. P.; Cross, J. B.; Bakken, V.; Adamo, C.; Jaramillo, J.; Gomperts, R.; Stratmann, R. E.; Yazyev, O.; Austin, A. J.; Cammi, R.; Pomelli, C.; Ochterski, J. W.; Ayala, P. Y.; Morokuma, K.; Voth, G. A.; Salvador, P.; Dannenberg, J. J.; Zakrzewski, V. G.; Dapprich, S.; Daniels, A. D.; Strain, M. C.; Farkas, O.; Malick, D. K.; Rabuck, A. D.; Raghavachari, K.; Foresman, J. B.; Ortiz, J. V.; Cui, Q.; Baboul, A. G.; Clifford, S.; Cioslowski, J.; Stefanov, B. B.; Liu, G.; Liashenko, A.; Piskorz, P.; Komaromi, I.; Martin, R. L.; Fox, D. J.; Keith, T.; Al-Laham, M. A.; Peng, C. Y.; Nanayakkara, A.; Challacombe, M.; Gill, P. M. W.; Johnson, B.; Chen, W.; Wong, M. W.; Gonzalez, C.; Pople, J. A. *Gaussian 03*, revision C.02; Gaussian, Inc.: Wallingford, CT, 2004.
(22) Kerr, K. A.; Ashmore, J. P. *Acta Crystallogr., Sect. B* **1975**, *31*, 2022−2026.
(23) Madden, J. J.; McGandy, E. L.; Seeman, N. C. *Acta Crystallogr., Sect. B* **1972**, *28*, 2377−2382.
(24) Foresman, J. B.; Frisch, A. *Exploring Chemistry with Electronic Structure Methods*, 2nd ed.; Gaussian, Inc.: Pittsburgh, PA, 1996.
(25) Bandekar, J.; Genzel, L.; Kremer, F.; Santo, L. *Spectrochim. Acta* **1983**, *39A*, 357−366.
(26) Okamoto, Y. *VXL*; Fuji Photo Film Co. Ltd., 2003.
(27) Kerr, K. A.; Ashmore, J. P. *Acta Crystallogr., Sect. B* **1973**, *29*, 2124−2127.